DEVELOPMENT OF INNOVATIVE FILTERING TECHNIQUES FOR IMPROVED DEPTH PHASE DETECTION AT REGIONAL DISTANCES

Delaine T. Reiter[1], Jessie L. Bonner[1], and Robert H. Shumway[2]

Weston Geophysical Corporation[1] and University of California, Davis[2]

Sponsored by National Nuclear Security Administration
Office of Nonproliferation Research and Engineering
Office of Defense Nuclear Nonproliferation

Contract No. DE-FG02-03ER83820

ABSTRACT

Accurate determination of the focal depth of seismic events continues to be an important seismic monitoring problem. The primary objective of this research is to improve seismic depth phase detection and identification capabilities at regional distances using new filtering techniques. To accomplish this objective, we applied wavelet denoising and optimal (Wiener) filtering to the problem of depth phase detection at regional distances for synthetic and real array data. We have developed a detection routine that includes array processing to isolate the *Pn* window for analysis, Fourier filtering and wavelet denoising of the windowed data to improve the signal-to-noise ratio (SNR), and depth phase analysis using a cepstral F-statistic detection module. We applied the processing routine to synthetic regional waveforms computed for an array of similar size and geometry to the South Korean seismic array (KSAR). Gaussian white and autoregressive (AR2) noise models were used to add complexity to the synthetic data, and many different simulations with variable signal-to-noise ratios were conducted to examine the performance of the filtering and denoising techniques on data. We concluded that wavelet denoising did not offer substantially improved detection rates over standard Fourier bandpass filtering if the depth phases were buried in white noise. However, when the waveforms were contaminated with noise produced by an AR2 model or observed noise from KSAR, we noted a significant decrease in the depth phase false alarm rate when wavelet denoising or Wiener filtering were applied.

These filtering techniques were then applied to a database of test events recorded at regional distances from the KSAR array. These events had high quality depth estimates that were based on multiple teleseismic depth phases. The KSAR array data were first processed using traditional *f-k* techniques to determine the analysis window, which typically includes pre-event noise, the *Pn* arrival, and the signal prior to *Pg* or other sustained arrivals with characteristics that differ from the *Pn* phase. We determined that a *sym4* wavelet decomposed at level 6 removed noise at periods less than 1 Hz better than the level-4 decomposition found in our synthetic studies. We applied the *sym4* wavelet, together with Heursure thresholding to denoise the events in our database and compared the results to those found using both standard Fourier filtering (Butterworth BP 0.6 to 4.5 Hz) and Wiener filtering. The results of this preliminary study suggest that wavelet denoising improves our ability to detect depth phases on complicated regional seismograms. Wavelet denoising improves our ability to visually detect phase arrival onset, but additionally, and perhaps more importantly, it decreases the false alarm rates in the cepstral F-statistic analysis significantly (by factors of 2 and greater). Our results thus far indicate that wavelet denoising is a feasible method that can improve the detectability and phase arrival time estimation of regional depth phases. Further study is needed to determine the effectiveness of the method in a data center/operational setting.

OBJECTIVES

The accurate estimation of the depth of small, regionally recorded events continues to be an important and difficult monitoring research problem. In our previous studies, we have focused on the extraction of depth phases from body waves using cepstral analysis (Bonner *et al*., 2002), with varied degrees of success at regional distances. The objective of the research presented in this paper is to improve the identification of regional seismic depth phases using innovative filtering techniques applied to the data prior to cepstral F-statistic processing.

RESEARCH ACCOMPLISHED

Seismologists are very familiar with filtering schemes based on Fourier analysis, which uses sine and cosine functions to represent seismograms. While this technique is highly effective in the analysis of seismic data, it has limitations when the signal contains sharp discontinuities or transient features. In contrast, wavelet analysis relies upon other classes of mathematical functions that can be used to dissect and represent data. The wavelet transform segments data into separate frequency components, which can then each be studied independently. For example, certain frequency components may consist of a large "window" of data that provides information on gross features of the data, while other frequency components allow the examination of smaller windows and detailed waveform features. Another advantage of the wavelet transform is that it can utilize many possible basis functions, while the Fourier transform has only one set of basis functions (sines and cosines). This allows wavelet analysis to illuminate features in the data that can be obscured by other time-frequency methods such as Fourier analysis. We refer the reader to additional references by Misiti *et al.* (2000), Strang and Nguyen (1996) and Daubechies (1992) for further background information on wavelets. In the following sections, we present the results of applying a type of wavelet analysis known as *wavelet denoising* to the problem of depth phase detection.

Development of Denoising Filters for Regional Seismograms

The objective in our application is to remove noise from regional seismic data, while retaining the complex depth phase signals. In previous research, we utilized Fourier band-pass filters to reduce noise and aid in the detection of depth phases. The results were not optimal at regional distances, and many false depth phase detections were attributed to background noise, secondary arrivals, and filtering artifacts. Therefore, we have applied various methods to wavelet denoise (Misiti *et al.*, 2000; Shumway and Stoffer, 2000) regional seismograms for improved depth phase extraction. The application of wavelet denoising requires the selection of three components: a wavelet basis function, the thresholding procedure and a noise scaling option. Each of these components is discussed below.

Wavelet Selection. The first step in producing a wavelet denoising filter is to choose a wavelet basis function to be used in decomposing the seismic waveforms. In our research we have focused on the *symmlet4* (or *sym4*) and *db2* wavelets, as described by Daubechies (1992), and the *bior3.5* wavelet (Tibuleac, 2003). We chose these wavelets based on their similarities to typical *P*-wave arrivals and their success in previous studies of *P* waves (Anant and Dowla, 1997; Tibuleac, 2003; Zhang *et al*., 2003). These wavelet functions are shown in Figure 1. Note that the *bior3.5* wavelet uses two different wavelets: one for decomposition and one for reconstruction

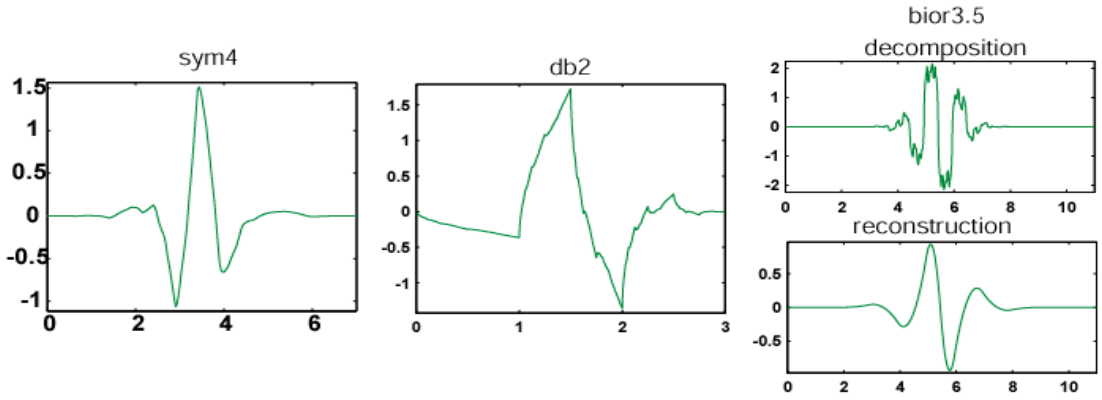

Figure 1. Wavelet basis functions used in the study.

Threshold Selection. To denoise a regional waveform, we must select a threshold that effectively removes seismic noise and increases the desired arrival (e.g., the depth phase) signal-to-noise ratio. The thresholding can be designated as either "hard" or "soft". Shumway and Stoffer (2000) provide a summary on how soft thresholding is accomplished. For example, the value of a wavelet detail coefficient, a, is set to 0 if $|a| \leq \lambda$, where λ is the actual threshold. For $|a| \geq \lambda$, the coefficient is set to some other value (e.g., $sign(a)(|a| - \lambda)$). In the case of hard thresholding, the coefficient is set to a if $|a| \geq \lambda$ and 0 if $|a| \leq \lambda$. Misiti *et al*. (2000) allow for several choices of thresholding, including methods known as Rigrsure, Sqtwolog, Heursure, and Minimaxi. We have compared these four methods of automatically determining a soft threshold; each is briefly described in Table 1.

Table 1. Threshold Selection Criteria (from Misiti *et al*., 2000)

Threshold Type	Comments
Minimax	Uses the Minimax principle (Mallat, 1999) to design estimators that realize the *minimum* of the *maximum* mean square error.
Rigrsure	Uses Stein's (1981) Unbiased Estimate of Risk to set a threshold that minimizes the risks.
Sqtwolog	Uses a Minimax threshold multiplied by a factor proportional to the log of the waveform length.
Heursure	Combines Sqtwolog and Rigrsure techniques.

Rescaling Options. The most basic noise model that we can consider consists of Gaussian white noise with $\sigma = 1$. However, this model is not often observed in practice, and more complex methods of rescaling the estimated noise function are necessary. We examined three different methods of scaling the noise in this study, including white noise with $\sigma = 1$ (i.e., rescaling is not performed), variable white noise, and non-white noise. They are briefly described in Table 2 and referred to throughout the study by their Misiti *et al*. (2000) descriptors.

Table 2. Noise Rescaling Options (from Misiti *et al*., 2000)

Method	Comments
ONE	No rescaling.
SLN	Rescales the noise based on coefficients in the first level of the wavelet decomposition.
MLN	Determines a rescaling factor estimated from noise at each decomposition level. Best used for non-white noise or signals where the noise changes characteristics at some time (t) in the data.

Application to Noisy Synthetics. The Herrmann (2002) wavenumber-integration code was used to generate synthetic seismograms for an array of seismometers with similar configuration to the first 11 elements of the KSAR (Wonju, South Korea) array (e.g., KS01-KS11). The IASP91 velocity model was used to generate these synthetics (Kennett and Engdahl, 1991). We simulated a double-couple earthquake at a depth of 15 km approximately 430 km from the array.

To examine the performance of wavelet denoising in different SNR conditions, we applied both Gaussian white and autoregressive noise of varying levels to the synthetic signals. For the autoregressive noise, we used observed seismic noise from the KSAR array (denoted $x(t)$) and a white noise input, $w(t)$, to calculate an autoregressive model of order 2 (AR2) with the equation (Shumway and Stoffer, 2000)

$$x(t) = x(t-1) - 0.90\ x(t-2) + w(t)\,. \qquad (1)$$

Our AR2 model estimates the current value of a time series as a scaled function of the previous two values of the series. This type of model is frequently used to model noise series in which periodic behavior is observed. Examples of both Gaussian white and AR2 noise are shown in Figure 2.

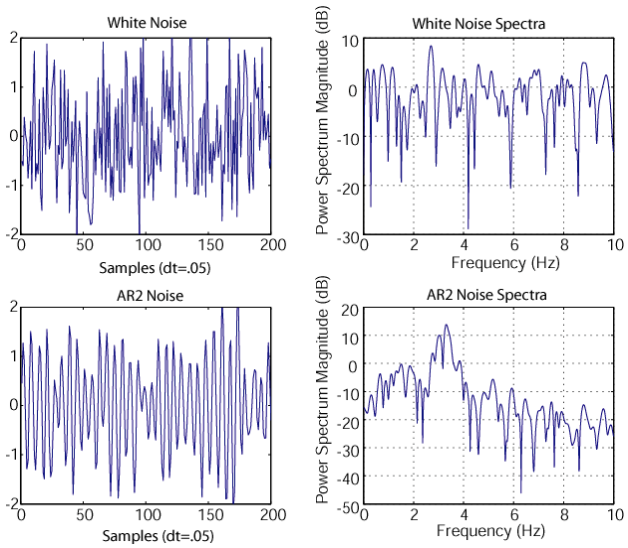

Figure 2. Examples of white and AR2 noise used in our evaluation of depth-phase denoising techniques. In practice, the amplitude of the noise was randomly scaled and added to the synthetic data.

Wavelet Denoising Results. We simulated 100 array recordings of the synthetic data using different Gaussian white or AR2 SNR levels ($0.7 < Pn$ SNR < 10). The synthetic data were windowed using traditional *f-k* techniques to determine an appropriate analysis window, which typically includes pre-event noise, the *Pn* arrival, and the signal prior to *Pg*. We then applied wavelet denoising using the wavelets shown in Figure 1, the thresholding routines listed in Table 1, and the rescaling options listed in Table 2. Figure 3 presents a comparison of wavelet denoising to standard Fourier filtering applied to a noisy regional signal containing depth phases.

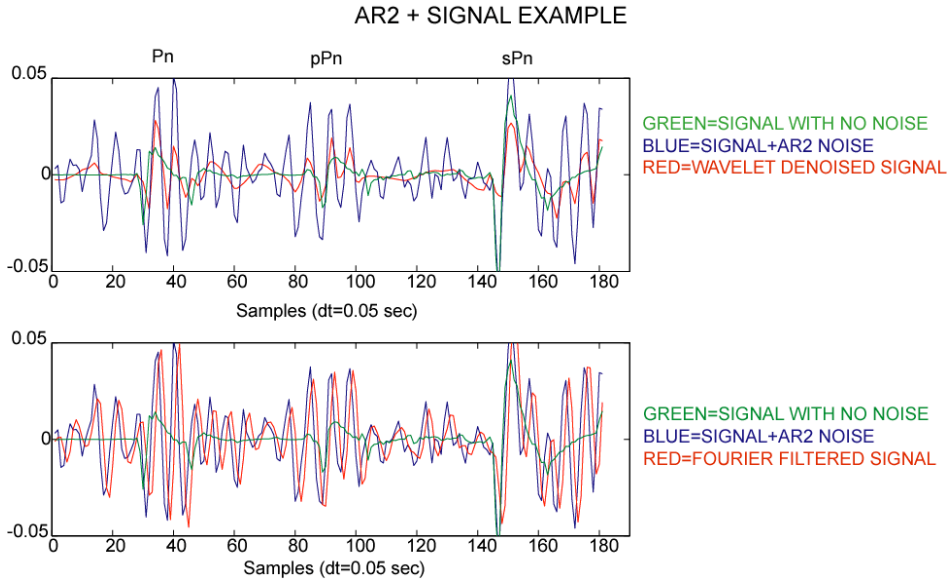

Figure 3. Comparison between wavelet denoising and Fourier filtering for synthetic *Pn*, *pPn*, and *sPn* arrivals contaminated with AR2 noise. (*Top*) Wavelet-denoised results (red), input noisy synthetic signal (blue), and noise-free synthetic signal (green). Wavelet denoising was performed using level-3 decomposition with the *sym4* wavelet, Heursure thresholding, and MLN rescaling. (*Bottom*) Fourier filtered results (red), input noisy synthetic signal (blue), and noise-free synthetic signal (green). We performed the Fourier filtering using a 3rd order band-pass filter (0.6 to 4.5 Hz).

To determine whether depth phase detection was improved by wavelet denoising compared to Fourier filtering, we input both the denoised and filtered waveforms into the cepstral F-statistic module of our depth phase processing tool (see Bonner *et al*., 2002), and potential depth phase candidates were selected. Figure 4 shows the results of the cepstral F-statistic processing for the case in which AR2 noise was added to the synthetic signals. These signals were then either Fourier filtered or wavelet denoised using all possible combinations of the processing options listed in Tables 1 and 2. The top plot in Figure 4 shows the ratio of the number of detections that were associated with the primary depth phases (hits; within ±0.25 seconds of IASP91-predicted depth phase arrival time) compared to the detections that were either artifacts of the filtering, noise-related, or multiple echoes (misses). The ratio for the Fourier filtering results is approximately 1.2 for the AR2 noise case. In contrast, the ratio for the wavelet-denoised data varies from as small as 1.2 to as high as 27 true detections per every false alarm. In the lower subplot the number of hits and misses per possible depth-phase candidate solutions is shown. The Heursure method of thresholding (see Table 1 for a description) with SLN rescaling consistently provides multiple successful hits and few misses at all decomposition levels when compared with the other results. The related Rigrsure method with SLN scaling also provides a high number of successful hits to misses. However, it is the Sqtwolog thresholding method using SLN rescaling that provides the highest success-to-failure ratios at all decomposition levels.

Although it not is shown here, we note that for white noise, the Heursure method of thresholding with SLN rescaling consistently provides the most successful hits and the least number of misses when compared with the other results. We also note, however, that the improvement offered by wavelet denoising over the Fourier filtering techniques is smaller than for the AR2 noise case.

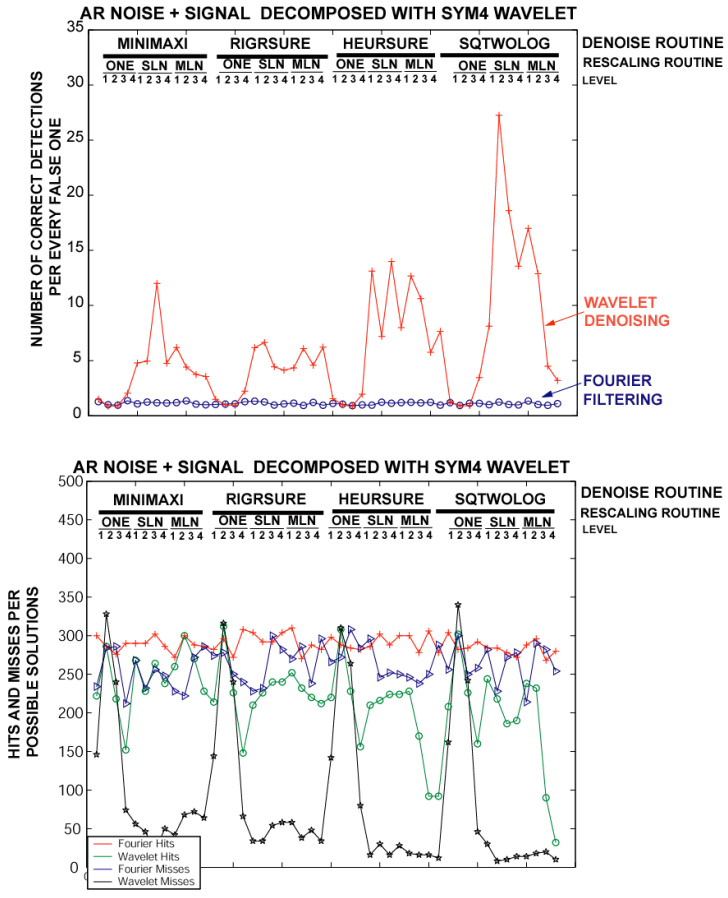

Figure 4. Cepstral F-statistic depth phase detection success to failure rates (top) and hits and misses (bottom) for standard Fourier filtering and wavelet denoising of synthetic data contaminated by AR2 noise. The denoising was accomplished using a sym4 wavelet at decomposition levels 1-4, thresholding routines including Minimax, Heursure, Rigrsure, and Sqtwolog, and rescaling models including ONE, SLN, and MLN. See Tables 1 and 2 for explanations.

Depth-Phase Detection Using Optimal (Wiener) Filtering. In the results presented thus far, we used a standard bandpass Fourier filter (0.6 to 4.5 Hz) that is frequently used in regional seismic applications. However, other types of Fourier filters are likely to be superior to the standard filtering technique. For example, we have compared the ability of wavelet denoising to find depth phases in noisy seismograms to that of an optimal (or Wiener) filter (Der and Shumway, 2000). To perform Wiener filtering, we place a 1.5-second "signal" window around the noisy synthetic *Pn* arrival and compute the Fourier transform of the signal and noise windows. We use the magnitude response for each of these windows and recursively design a filter to match these spectra. This Wiener filter is then applied to the noisy data and the result input into the cepstral F-statistic for depth phase analysis.

The results indicate that use of the Wiener filter improves success-to-failure rates for depth phase detections in white noise compared to wavelet denoising and standard Fourier filtering. This improved detection rate is a result of fewer false alarms, but comes at the expense of fewer detections. When AR2 noise is added to the signal, the Wiener filter again provides increased performance over the standard Fourier filtering. Also, wavelet denoising and Wiener filtering have similar false alarm rates for the AR2 noise case; however, the wavelet denoising results in increased detections of depth phases. Overall, these results suggest that Wiener filters can be designed that compete with wavelet denoising in terms of improved depth-phase detection capabilities.

Denoising Applied to Regional KSAR Data for Improved Depth Phase Detection

We applied the standard Fourier, wavelet denoising and Wiener filtering techniques to a small test data set of regional waveforms recorded at the South Korean seismic array (KSAR). We determined the optimum denoising parameters for these data and examined the extent to which the new filtering methods increase depth phase detection capabilities. We note that for this phase of the project, our focus was not on blind testing of the method. Our objective was to determine if the denoising procedure could improve depth phase detection, which dictated that we know *a priori* where the depth phase detections actually occurred. In the following sections, we present depth-phase detection results from two events in this waveform database. Further analysis will be completed during future research on this project.

Honshu, Japan. The first example is an event with m_b=4.7 from the Honshu region of Japan, located by the preliminary International Data Center (pIDC) at a depth of 22 km (based on multiple teleseismic depth phase arrivals). The event occurred approximately due east of KSAR at an epicentral distance of 10.2 degrees (Figure 5A). Although KSAR has 19 short-period elements, we processed a subset of the first 11 elements (Figure 5B) to imitate the number of short-period elements in prototype regional arrays that have recently been installed in important monitoring regions. The *Pn* arrival for this event at KSAR has large SNR (Figure 5C); however, the signal-generated noise is also large and may be obscuring the possible depth phases. *F-K* array processing (Figure 5D) on the first 25 seconds of data following the initial *P*-wave suggests there is no clear *Pb* or *Pg* arrival, thus the depth-phase analysis includes 25-second windows of both noise and signal.

We performed cepstral F-statistic analyses on these data following wavelet denoising (Figure 6A), standard Fourier filtering (Figure 6B), and Wiener filtering (Figure 6C). The array beam resulting from the application of these filtering/denoising techniques is presented in the upper subplot of each cepstral analysis. In the lower subplots, the cepstral F-statistic analysis is time aligned to the *P*-wave arrival. The initial 2 seconds of cepstral results are not plotted, because large amplitude peaks caused by non-varying direct current (DC) offsets that occur in the log spectra. For the wavelet denoising, we used Heursure thresholding and a *sym4* wavelet decomposed at level 6. The Fourier filtering was accomplished using a Butterworth bandpass filter between 0.6 and 4.5 Hz, and the Wiener filtering was completed by centering a 1.5-second signal window on the *Pn* arrival. The IASP91-predicted travel time arrivals for this event are shown above the top subplot in each of these analyses.

We note that wavelet denoising produces clean waveforms that highlight the regional depth phases. Additionally, cepstral F-statistic results for the denoised data shows a very large peak that corresponds to the *pPn* arrival and a smaller statistically significant peak (at a 99% significance level) for the *sPn* arrival. For the wavelet denoising results, we only note two additional peaks that do not correspond to the predicted arrival of the depth phases (i.e., false detections). The standard Fourier and Wiener filtering also detect the depth phases; however, the number of false detections is up by a factor of three over the wavelet-denoised data. The improvement in success to failure rates noted on these real data are similar to the rates observed from the analysis of the synthetic data presented earlier.

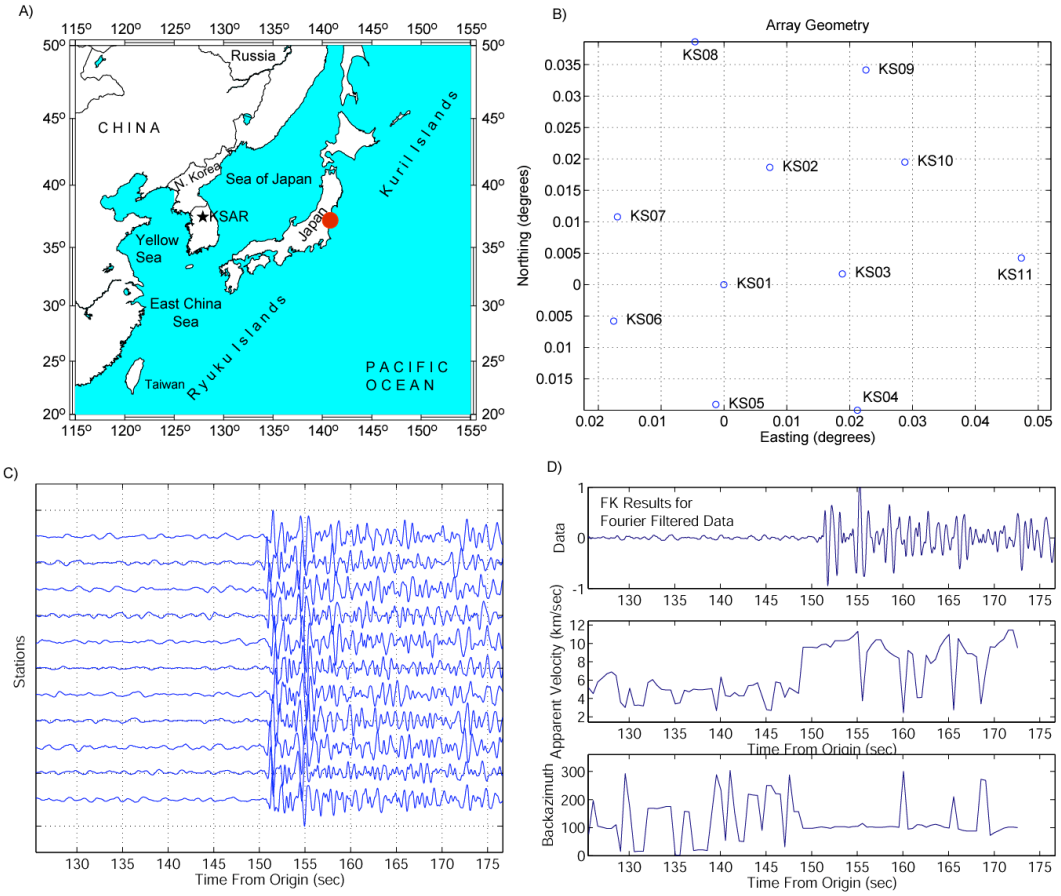

Figure 5. Array processing for Honshu, Japan event (pIDC EVID 1259474). A) Location of event and KSAR array. B) KSAR elements used in the processing. C) Unfiltered seismic records for KSAR stations shown in subplot B. D) *f-k* results showing sample data, phase velocity, and backazimuth. The *f-k* results are used to pick the analysis window.

Kuril Islands. The second example presented is an m_b=4.5 event from the Kuril Islands, located by the pIDC at a depth of 30.1 km and 16.6 degrees northeast of KSAR (Figure 7A). KS01 was not available for this event, so we show only 10 elements in Figure 7B, with KS02 as the new reference station. The *f-k* array processing (Figure 7D) reveals a slowly-propagating, off-azimuth arrival near 250 seconds and a fast arrival near 255 seconds after origin (with a 4-second window length in the *f-k* analysis). To avoid contamination from these arrivals, which may or may not be associated with the event of interest, the cepstral analysis window was ended prior to these arrivals. The results of the cepstral analysis are shown in Figure 8, and we note that wavelet denoising best highlights the regional depth phases. The cepstral F-statistic results for the wavelet-denoised data show a large peak that corresponds to the *pPn* arrival; however, the peak for the *sPn* arrival is not statistically significant at the 99% level. The Wiener filtering method also detects the *pPn* depth phase and two false detections, while standard Fourier filtering had no correct depth phase detections.

CONCLUSIONS AND RECOMMENDATIONS

Accurate estimation of the depth of small, regionally recorded events continues to be an important and difficult monitoring research problem. In our previous studies we have focused on the extraction of depth phases from body waves, with varied degrees of success at regional distances. In this paper, we demonstrated that wavelet denoising shows promise in improving depth phase detectability on complex regional seismograms. To further enhance regional focal depth estimation accuracy, we believe other technologies that utilize different features of the seismic waveform must be exploited. Therefore, the primary goal of the next stage of our project will be to develop a

synergistic tool that combines three different methods to estimate the depth of regional seismic events. These methods include 1) improved depth phase detection in the complex *Pn* coda of regional seismograms; 2) sparse-network hypocenter locations with associated Monte-Carlo confidence regions that incorporate regional primary and depth phase arrivals; and 3) surface-wave spectral amplitude inversions for depth. We will then use rigorous statistical analyses to combine these three different methods into a depth and associated confidence estimate.

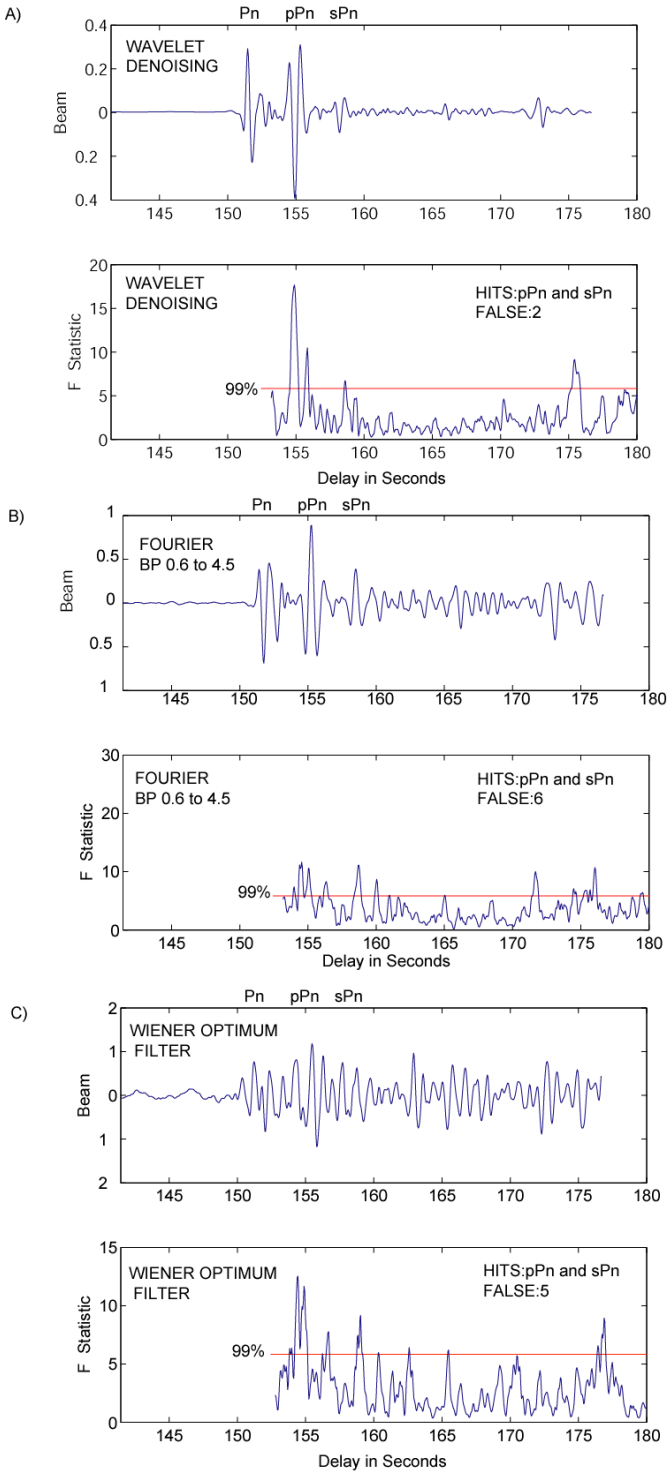

Figure 6. Cepstral F-Statistic processing for the Honshu, Japan event (pIDC EVID 1359474). A) *Top*: Array beam of wavelet-denoised data. The IASP91 predicted times of the depth phases are indicated above the top subplot. *Bottom*: Results of applying the cepstral F-statistic method to wavelet-denoised data (red line is the 99% significance level). The cepstral F-statistic is time aligned to the *P*-wave arrival; the initial 2 seconds of cepstral results are not plotted due to large amplitude peaks caused by a DC offset in the spectra. B) *Top*: Array beam of Fourier-filtered data. *Bottom*: Results of applying the cepstral F-statistic method to standard Fourier-filtered data. C) *Top*: Array beam of Wiener-filtered data. *Bottom*: Results of applying cepstral F-statistic method to Wiener-filtered data.

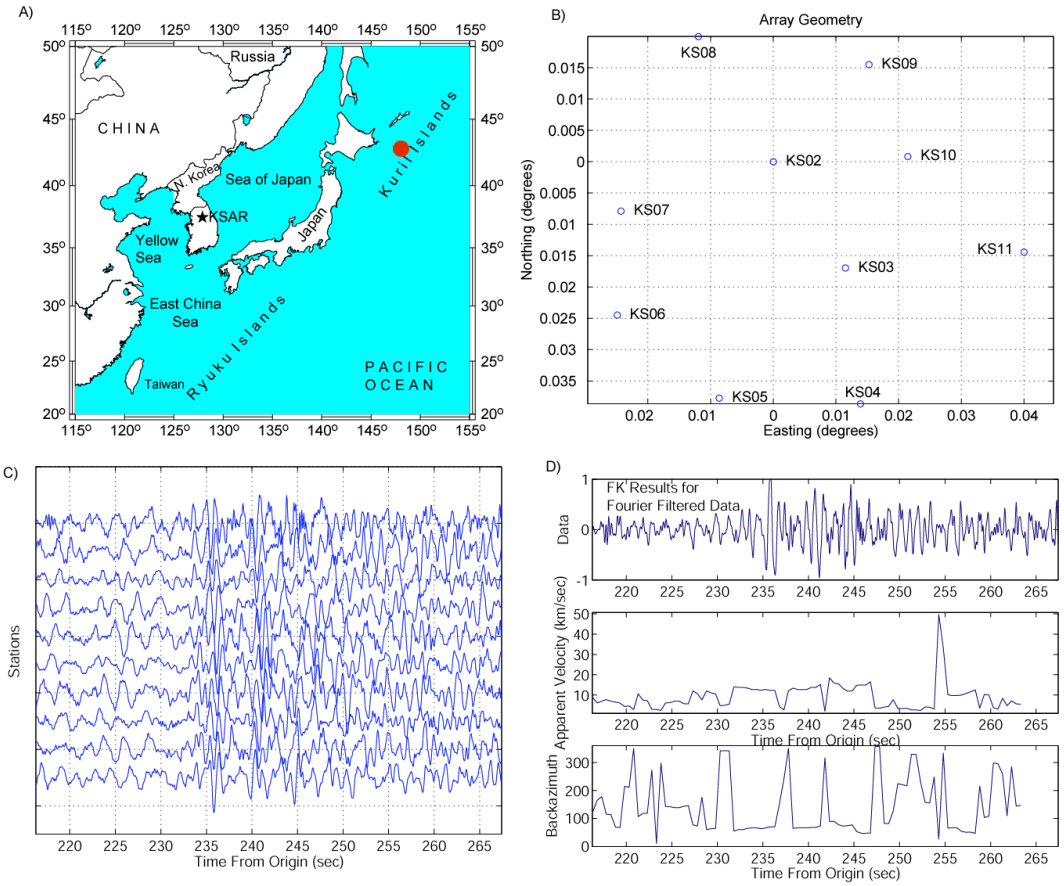

Figure 7. Array processing for Kuril Islands event (pIDC EVID 21380185). A) Location of event and KSAR array. B) KSAR elements used in the processing. C) Unfiltered seismic records for KSAR stations shown in subplot B. D) *F-K* array processing results showing sample data, phase velocity, and backazimuth.

REFERENCES

Anant, K. S. and F. U. Dowla (1997), Wavelet transform methods for phase identification in three-component seismograms, *Bull. Seis. Soc. Am.*, 87, 1598-1612.

Bonner, J. D.T. Reiter, and R. H. Shumway (2002), Application of a cepstral F statistic for improved depth estimation, *Bull. Seism. Soc. Am*, 92, 1675-1693.

Daubechies, I. (1992), Ten lectures on wavelets, *Regional Conference Series in Applied Mathematics*, Vol. 61.

Der, Z. and R. H. Shumway (2000), Automatic interpretation of regional seismic signals using the CUMSUM-SA algorithms, *Proceedings* of the 21st Annual Seismic Research Symposium on Monitoring a Comprehensive Nuclear Test Ban Treaty, 393–403.

Herrmann, R. B. (2002), Computer Programs in Seismology Version 3.15, St. Louis University.

Kennett B. L. N., and E. R. Engdahl (1991), Travel times for global earthquake location and phase identification, *Geophys. J. Int.,* 105, 429-465.

Mallat, S. (1999). A Wavelet Tour of Signal Processing. Academic, San Diego, 2nd edition.

Misiti, M., Misiti, Y., Oppenheim, G. and J. Poggi, (2000), *Wavelet Toolbox*, *ForUse with Matlab*, © Copyright 1996 by the MathWorks, Inc.

Shumway, R. H., and D. S. Stoffer (2000), Time Series Analysis and its Applications. Springer Verlag.

Strang, G., and T. Nguyen (1996), *Wavelets and Filter Banks*, Wellesley-Cambridge Press.

Tibuleac, I.M. (2003). Wavelet pre-processing for stable magnitude estimation and spectral mb magnitudes. Weston Geophysical Scientific Report

Zhang, H., C. Thurber and C. Rowe (2003), Automatic P-wave arrival detection and picking with multiscale wavelet analysis for single-component recordings, *Bull. Seism. Soc. Am.,* 93, 1904 – 1912.

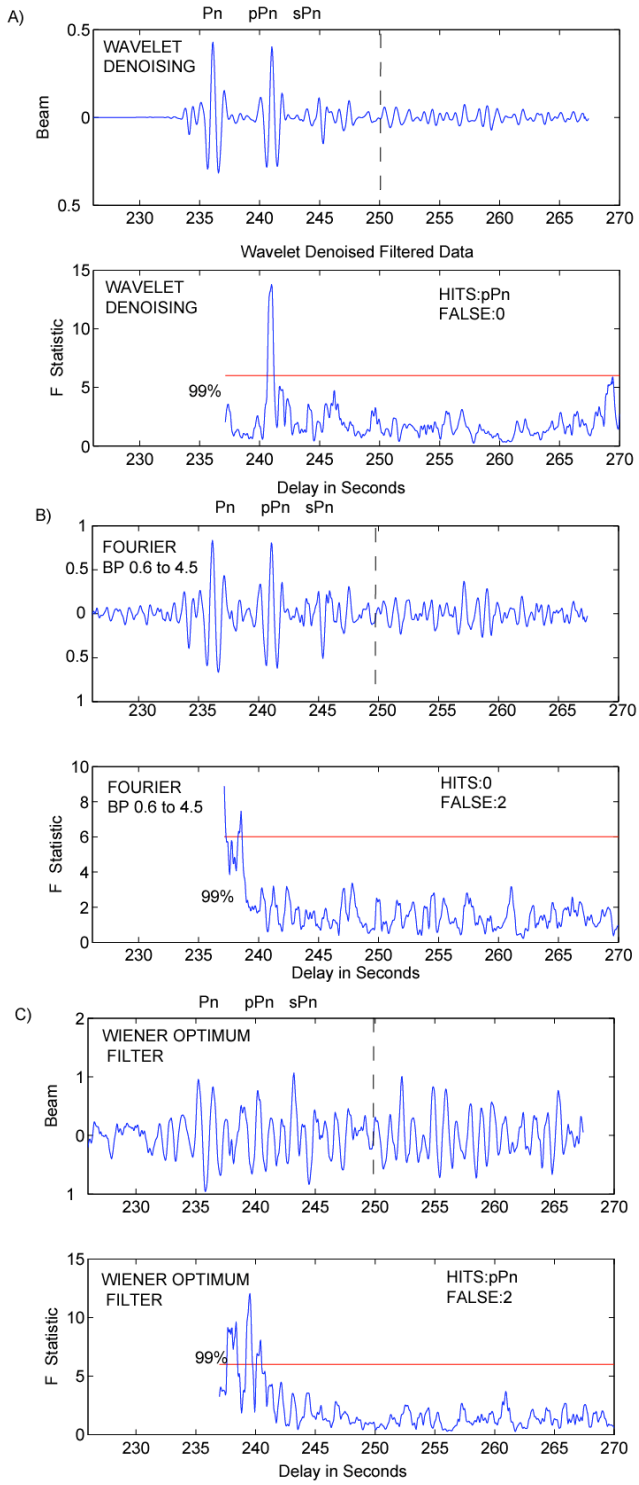

Figure 8. Cepstral F-Statistic processing for Kuril Islands event (pIDC EVID 21380185). A) *Top*: Array beam of wavelet-denoised data. The IASP91 predicted times of the depth phases are indicated above the top subplot. The dashed line shows the end of the cepstral analysis window. *Bottom*: Results of applying the cepstral F-statistic method to wavelet-denoised data (red line is the 99% significance level). The cepstral F-statistic is time aligned to the *P*-wave arrival; the initial 2 seconds of cepstral results are not plotted due to large amplitude peaks caused by a DC offset in the spectra. B) *Top*: Array beam of Fourier-filtered data. *Bottom*: Results of applying the cepstral F-statistic method to standard Fourier-filtered data. C) *Top*: Array beam of Wiener-filtered data. *Bottom*: Results of applying cepstral F-statistic method to Wiener-filtered data